# Mechanical Blocking Mechanism for the Columnar to Equiaxed Transition

V.B. BISCUOLA and M.A. MARTORANO

Mechanical blocking of the columnar front during the columnar to equiaxed transition (CET) is studied by quantitatively comparing the CET positions obtained with one stochastic model and two deterministic models for the unidirectional solidification of an Al-7 (wt pct) Si alloy. One of the deterministic models is based on the solutal blocking of the columnar front, whereas the other model is based on the mechanical blocking. The solutal-blocking model and the mechanical-blocking model with the traditional blocking fraction of 0.49 give columnar zones larger than those predicted with the stochastic model. When a blocking fraction of 0.2 is adopted, however, the agreement is very good for a range of nucleation undercoolings and number density of equiaxed grains. Therefore, changing the mechanical-blocking fraction in deterministic models from 0.49 to 0.2 seems to model more accurately the mechanical-blocking process that can lead to the CET.

DOI: 10.1007/s11661-008-9643-x


## I. INTRODUCTION

IN the as-cast macrostructure of a casting, the transition from columnar to equiaxed grains is called the columnar to equiaxed transition (CET). The CET position determines the amount of columnar and equiaxed grains, which strongly affects the properties of castings. Different mechanisms have been proposed to explain the CET during solidification, but it is generally accepted that it occurs when equiaxed grains block the growth of columnar grains.[1–3] Therefore, mathematical models to predict the position of the CET have usually considered the growth of both columnar and equiaxed grains.

One of the first mathematical models to predict the CET was proposed by Hunt,[4] who assumed unidirectional steady-state solidification. In this model, equiaxed grains nucleate at a prescribed nucleation temperature and grow in the constitutionally undercooled zone ahead of the growing columnar front. To determine the CET, Hunt[4] considered that the moving columnar front would be blocked when the volume fraction of equiaxed grains growing ahead was larger than 0.49. This criterion, which was later called the mechanical-blocking criterion,[5] hinges upon the concept that columnar grains would be blocked if they were unable to grow along a distance larger than the equiaxed-grain diameter.[4] Although the 0.49 fraction has never been questioned, it has been adopted in numerous deterministic models to predict the CET.[6–10]

V.B. BISCUOLA, Graduate Student, and M.A. MARTORANO, Professor, are with the Department of Metallurgical and Materials Engineering, University of São Paulo, Av. Prof. Mello Moraes, 2463 São Paulo-SP, 05508-900, Brazil. Contact email: martoran@usp.br
Manuscript submitted on February 26, 2008.
Article published online September 11, 2008

In the extension of the model of Wang and Beckermann,[8] proposed by Martorano *et al.*,[5] no criterion was necessary to predict the columnar-front blocking and the CET. In this model, the columnar front was automatically blocked (causing the CET) when the solute rejected by the equiaxed grains growing ahead of the front decreased the undercooling available for dendritic growth. Nguyen-Thi *et al.*[3] have presented some *in-situ* X-ray radiographic images of dendritic solidification in an Al-3.5 pct Ni alloy that confirm this effect, referred to as solutal blocking. Nevertheless, these images were obtained for solidification in a thin container (150 to 200 $\mu$m in thickness), whose walls might have affected the columnar-front blocking, as shown by Mathiesen and Arnberg[11] and Mathiesen *et al.*[12]

Ludwig and Wu[13] and Ciobanas *et al.*[14] considered both mechanical and solutal blockings in their models, suggesting that the two blocking mechanisms should play an important role in causing the CET. Browne[15] proposed an equiaxed index based on the time evolution of the liquid undercooling ahead of the columnar front. When this index reached its maximum value, Browne[15] assumed that the CET would occur. Banaszek *et al.*[16] observed that, in the presence of natural convection in the liquid, the index increased approximately twice, enhancing conditions for the CET.

A third type of blocking, denoted as thermal blocking, was shown by Banaszek *et al.*[16] and Mc Fadden and Browne[17] to occur. Banaszek *et al.*[16] used the model proposed by Browne and Hunt[18] to simulate the solidification of an Al-2 pct Cu alloy and showed that the columnar-front velocity began to decrease and eventually stopped, owing to the thermal interactions with equiaxed grains growing ahead of the front.

The aforementioned models are defined as deterministic. Another type of CET model denoted as stochastic was initially developed from the Monte Carlo concept.[19] Stochastic models, which always have a random

variable in their equations, calculate an image of the grain macrostructure, in which the CET occurs naturally without definition of any blocking criterion to stop the columnar front. These pioneering stochastic models evolved into the popular cellular-automaton finite-element (CAFE) model proposed by Gandin and Rappaz,[20] which is based on the cellular-automaton technique to simulate the nucleation and growth of grains. The CET identified visually in the CAFE macrostructures were compared with that observed experimentally, showing good agreement.[21] The cellular-automaton model was further developed, originating the so-called modified cellular-automaton models, as proposed by Dong and Lee.[22] In these models, the cellular-automaton technique is applied at the length scale of the dendrite arms, rather than the length scale of the grain envelopes, as in CAFE. Therefore, in the modified cellular-automaton models, the growth of dendrite arms and the advance of dendrite tips are simulated.

The implementation of the mechanical blocking of the columnar front in deterministic models of the CET requires the definition of a blocking fraction. A blocking fraction of 0.49 has been frequently used but has never been experimentally verified because the nucleation undercooling is also unknown in the model and has to be estimated. Therefore, a comparison between experiments and model results would only enable a combination of blocking fraction and nucleation undercooling to be determined, rather than the blocking fraction alone.

Calculating grain macrostructures with a stochastic model requires the definition of only the nucleation undercooling, because the mechanical blocking of the columnar front occurs automatically, without the need for any blocking fraction. Consequently, if both stochastic and deterministic models were used to calculate the CET position for the same nucleation undercooling, the mechanical-blocking fraction for the deterministic model could be obtained independently to give the best agreement between their results. Because the CET observed in macrostructures calculated with the stochastic models, especially those that employ the CA technique, are in good agreement with the actual CET,[23–26] the blocking fraction derived from the comparison is likely to be a good estimate of the actual fraction.

The aim of the present work is to investigate the mechanical blocking of the columnar front leading to the CET. The mechanical-blocking fraction is examined by quantitatively comparing the CET obtained from the macrostructures calculated with a stochastic model and the CET obtained with two deterministic models for a unidirectional-solidification system. The stochastic model is based on the CA technique; one of the deterministic models is based on the mechanical blocking of the columnar front, and the other, on the solutal blocking. Although the present analysis is focused on the mechanical-blocking mechanism, results from the solutal-blocking model are also given because experimental evidence of its importance has been revealed recently.[3] Note that the two blocking mechanisms, *i.e.*, mechanical and solutal, are implemented independently in the models of the CET.[13,14] For example, in the model of Wu and Ludwig,[27] the two blocking mechanisms were implemented to work simultaneously because in certain solidification conditions either one or the other causes the columnar-front blocking. The mechanical-blocking mechanism is strongly dependent on the geometry and growth kinetics of the columnar and equiaxed grains (which depends, for example, on the cooling rate, alloy composition, and inoculation of the alloy) and can be examined in a separate investigation, which is the objective of the present work.

## II. DESCRIPTION OF STOCHASTIC AND DETERMINISTIC MATHEMATICAL MODELS

One stochastic model based on the CA technique and two deterministic models were implemented in the present work to simulate the unidirectional solidification of an Al-7 (wt pct) Si alloy. These models will be only briefly described here because their details are available in the literature.

### A. *Stochastic Model*

The stochastic model is virtually identical with the CAFE model proposed by Gandin and Rappaz,[20] consisting of a macroscopic and a microscopic submodel and the coupling between them. The only difference is the use of the explicit finite-volume method,[28] rather than the finite-element method adopted in CAFE, to solve the heat-conduction equation of the macroscopic submodel. The equation is as follows:

$$\frac{\partial H}{\partial t} = \frac{\partial}{\partial y}\left(\kappa \frac{\partial T}{\partial y}\right) \qquad [1]$$

where $H$ is the volumetric enthalpy; $T$ is the temperature; $t$ is time; $y$ is the spatial coordinate in the direction of the heat flow; and $\kappa$ is the thermal conductivity, defined as an average of the liquid and solid conductivities weighted by their corresponding volume fractions. This equation was discretized by a one-dimensional (1-D) mesh consisting of one row of rectangular finite volumes aligned in the $y$ direction. Note that each volume has one node at the center and exchanges heat only through the two faces in contact with neighbor volumes.

The microscopic submodel was developed to simulate the nucleation and growth of dendritic grains in two dimensions. A two-dimensional (2-D) numerical mesh of CA square cells with a CA site at each cell center was used. Some of the cells contained substrate particles for heterogeneous nucleation of grains. The total number of particles randomly distributed among the cells was calculated from an average number density, $n_T$. The undercooling for nucleation on a particle was $\Delta T_N = T_L - T_N$, where $T_L$ and $T_N$ denote the liquidus and nucleation temperatures, respectively. In the present work, an instantaneous nucleation model was considered, *i.e.*, all substrate particles have the same nucleation undercooling, $\Delta T_N$.

To simulate the growth of dendritic grains, a square was associated with each CA cell, and its diagonals grew at a velocity, $V_d$, given as follows:[20]

$$V_d = A\Delta T^m \quad [2]$$

where $\Delta T$ is the undercooling ($\Delta T = T_L - T$) at the cell site position; and $A$ and $m$ are constants that depend on the alloy. The temperature, $T$, at the cell site is calculated by an interpolation of the $T$ values calculated at the finite-volume nodes of the macroscopic submodel. Because the finite volumes only exchange heat in the $y$ direction, the interpolated temperature is equal at all CA cells perpendicular to the $y$ direction.

The coupling between the macroscopic and microscopic submodels was implemented exactly as in the CAFE model. After a time-step of the numerical method, the change in volumetric enthalpy calculated at the nodes by the macroscopic submodel is interpolated at the position of the cell sites in a method similar to the temperature interpolation. The change in solid fraction at the cell sites during one time-step is obtained from this interpolated enthalpy change, assuming the Scheil model within each cell. Therefore, according to the Scheil model, no solute is transferred into or out of the cells or envelopes. The changes in solid fraction obtained for all cells within a finite volume are averaged to give the solid fraction change at the finite-volume nodes of the macroscopic submodel, allowing calculation of $\partial\varepsilon_s/\partial t$. The coupling cycle ends, and the temperature of the node is finally calculated by the discretized form of the following equation:

$$\rho c_P \frac{\partial T}{\partial t} = \frac{\partial H}{\partial t} + \rho L_f \frac{\partial \varepsilon_s}{\partial t} \quad [3]$$

where $c_p$ is the specific heat, $\rho$ is the density, $L_f$ is the latent heat of fusion, and $\varepsilon_s$ is volume fraction of solid. Note that $\partial H/\partial t$ is known from Eq. [1].

Further details of this coupling are in the literature.[20] As a validation step, some results of the implemented model were compared with those presented by Rappaz and Gandin,[29,30] showing very good agreement.

## B. *Deterministic Models*

Two deterministic models, each with a different mechanism for columnar-front blocking, were implemented: the model proposed by Martorano *et al.*[5] (MBG), which is an extension of the Wang and Beckermann[8] model, to consider the solutal blocking, and a model derived by modifying Hunt's[4] model (MHunt), considering the mechanical blocking. Both these models are based on the concept of a representative elementary volume (REV) containing many grain envelopes,[8,31] which are imaginary surfaces touching the tips of primary- and secondary-dendrite arms. As proposed by Wang and Beckermann,[8] three pseudophases are identified in the REV: solid ($s$), interdendritic liquid ($d$), and extradendritic liquid ($l$). The interdendritic- and extradendritic-liquid phases are the liquid inside and outside the grain envelopes, respectively.

The governing equations of the deterministic models were derived from the principles of mass, species, and energy conservation considering the following assumptions:[5,8] (a) melt flow, movement of solid, solute diffusion in the solid, and macroscopic diffusion in the liquid are negligible; (b) all possible equiaxed grains, determined by the number density, $n_T$, nucleate in the liquid when a local-nucleation undercooling, $\Delta T_N$, is reached (instantaneous nucleation); (c) the temperature is uniform inside a REV; (d) the specific heats, $c_p$, and the densities, $\rho$, of the pseudophases are equal and constant; (e) the thermal conductivity, $\kappa$, is calculated from $\kappa = \varepsilon_s\kappa_s + (\varepsilon_d + \varepsilon_l)\kappa_l$, where $\varepsilon$ represents the volume fraction and the subscripts indicate the pseudophases; and (f) the solute concentration in the interdendritic liquid, $C_d$, is uniform within the REV and is related to the temperature, $T$, by the liquidus line of the phase diagram, *i.e.*, $T = T_f + m_l C_d$, where $T_f$ is the melting point of the pure metal and $m_l$ is the slope of the liquidus line.

Based on these assumptions, the set of equations that are common to the two deterministic models are given as follows:

$$\rho c_P \frac{\partial T}{\partial t} = \frac{\partial}{\partial y}\left(\kappa \frac{\partial T}{\partial y}\right) + \rho L_f \frac{\partial \varepsilon_s}{\partial t} \quad [4]$$

$$\frac{\partial \varepsilon_g}{\partial t} = -\frac{\partial \varepsilon_l}{\partial t} = S_e V \quad [5]$$

$$\varepsilon_s + \varepsilon_d + \varepsilon_l = 1 \quad [6]$$

where $\varepsilon_g$ is the volume fraction of grain envelopes, defined as $\varepsilon_g = \varepsilon_s + \varepsilon_d = 1 - \varepsilon_l$; $S_e$ is the surface area of grain envelopes per unit volume; and $V$ is the radial-growth velocity of the cylindrical columnar and spherical equiaxed envelopes. This velocity is calculated by the Lipton–Glicksmann–Kurz model[5,8,32] as follows:

$$V = \frac{D_l m_l (k-1) C_d}{\pi^2 \Gamma}\left[0.4567\left(\frac{\Omega}{1-\Omega}\right)^{1.195}\right]^2 \quad [7]$$

where $\Gamma$ is the Gibbs–Thomson coefficient; $D_l$ is the diffusion coefficient of solute in the liquid; $k$ is the solute-partition coefficient; and $\Omega$ is a dimensionless undercooling, defined as follows:

$$\Omega = \frac{C_d - C_l}{C_d(1-k)} \quad [8]$$

where $C_l$ is the solute concentration in the extradendritic liquid.

The envelope surface-area concentration, $S_e$, is calculated as follows:[5,8]

$$S_e = \psi \frac{3(1-\varepsilon_l)^{\frac{2}{3}}}{R_f} \quad [9]$$

where $\psi$ is a correction factor for the effect of grain impingement (defined in Sections 1 and 2); and $R_f$ is a characteristic half spacing between envelopes, defined as

$R_f = \left(\frac{3}{4\pi n_T}\right)^{1/3}$ for equiaxed grains and $R_f = \lambda_1/2$ for columnar grains. In these equations, $n_T$ is the number density of equiaxed grains, and $\lambda_1$ is the dendrite-primary arm spacing within columnar grains. The position of the columnar front was tracked by numerically solving the following equation:

$$\frac{dy_{\text{col}}}{dt} = V \qquad [10]$$

where $y_{\text{col}}$ is the columnar-front position, and $V$ is the columnar-front velocity, calculated by Eq. [7], using $\Omega$ interpolated at the front position.

When the calculated local temperature, $T$, reaches the eutectic temperature, $T_E$, the eutectic reaction begins locally, and the energy-conservation equation (Eq. [4]) is now used to calculate the solid fraction, $\varepsilon_s$, rather than $T$. Equations [4] through [10] are used for both the MBG and MHunt models. In the following sections, the equations specific to each model are presented.

1. *Modified Hunt model—mechanical blocking*

As assumed in the model presented by Hunt,[4] the solid fraction within grain envelopes (internal solid fraction) is related to the interdendritic-liquid concentration, $C_d$, by the Scheil equation. This assumption leads to the following governing equation to calculate the time rate of the total solid-fraction change in the REV:

$$\frac{\partial \varepsilon_s}{\partial t} = \frac{\varepsilon_d}{(1-k)C_d}\frac{\partial C_d}{\partial t} + S_e V\left(1 - \left(\frac{C_d}{C_0}\right)^{\frac{1}{k-1}}\right) \qquad [11]$$

where $C_0$ is the average solute concentration of the alloy. The rate of solid-fraction change, $\partial\varepsilon_s/\partial t$, comprises a change in the solid fraction owing to columnar- and equiaxed-grain solidification.

The internal solid fraction within grain envelopes, given by $\varepsilon_s/\varepsilon_g$, was assumed to follow the Scheil equation, implying that no solute is exchanged between the envelopes and the surrounding liquid (extradendritic liquid). In other words, the average solute concentration of each envelope (considering solid and interdendritic liquid) and of the surrounding liquid ($C_l$) are kept constant at $C_0$ during solidification. Accordingly, $C_l = C_0$ in Eq. [8].

Grains are assumed to nucleate at random locations in the extradendritic liquid, as in Hunt's[4] model. Therefore, the Avrami correction was used to consider the effect of grain impingement during growth, implying that $\psi = \varepsilon_l$ in Eq. [9].

Finally, to complete MHunt model, it was assumed that the columnar front was blocked, causing the CET, when the equiaxed grain fraction at the front was equal to or larger than a predetermined blocking fraction (mechanical blocking). Two blocking fractions were examined: 0.49 (MHunt-0.49), as assumed in the original Hunt[4] model, and 0.2 (MHunt-0.2).

2. *MBG model—solutal blocking*

The model of the CET proposed by Martorano *et al.*,[5] which uses a solutal-blocking mechanism of the columnar front, was implemented. In contrast with the MHunt and stochastic models, the exchange of solute between grain envelopes and the extradendritic liquid was taken into account using the differential equations proposed by Wang and Beckermann.[8] The following equations were finally adopted to respectively calculate the solid fraction, $\varepsilon_s$, and the solute concentration of the extradendritic liquid, $C_l$:

$$(1-k)\,C_d\frac{\partial \varepsilon_s}{\partial t} = \varepsilon_d\frac{\partial C_d}{\partial t} + S_e\frac{D_l}{\delta_e}(C_d - C_l) \qquad [12]$$

$$\frac{\partial(\varepsilon_l C_l)}{\partial t} = C_d\frac{\partial \varepsilon_l}{\partial t} + S_e\frac{D_l}{\delta_e}(C_d - C_l) \qquad [13]$$

where $\delta_e$ is the effective diffusion length in the liquid adjacent to the grain envelopes, calculated as in the MBG model. Now, $C_l$ is not constant, as opposed to the MHunt model, in which $C_l$ remained equal to $C_0$ during solidification. Its value changes with time, decreasing the undercooling for the growth of equiaxed and columnar grains and causing the CET without any external front-blocking criterion. The Avrami correction was not originally used in the MBG model; therefore, $\psi = 1$ in Eq. [9].

The system of coupled equations for the MHunt and MBG models were solved numerically using the implicit formulation of the finite-volume method.[5,28] To discretize the differential equations, the calculation domain was subdivided into a 1-D mesh of finite volumes with centered nodes.

## III. ASPECT RATIO CRITERION TO DETERMINE THE CET

The CET positions predicted with the stochastic and the two deterministic models were compared. The CET position was obtained directly from the equations of the deterministic models, whereas a criterion based on the aspect ratio of grains was used to determine the CET position from the 2-D macrostructures calculated with the stochastic model.

The aspect ratio of a grain was determined by first obtaining the length, $L_1$, of the longest straight-line segment possible to be inscribed within the grain, considering all line orientations. Next, the length, $L_2$, of the longest line inscribed within the grain and orthogonal to the first line was obtained. The aspect ratio was finally defined as $\phi = \frac{L_2}{L_1}$, as presented by Allen[33] to characterize the shape of particles in image-analysis systems.

To investigate the effect of the CA mesh on the aforementioned procedure, values of $\phi$ were determined for an ellipse of actual $\phi = 0.6$, represented in CA meshes of different sizes and relative orientations. The results given in Figure 1(a) indicate that the error is 1.3 pct for a mesh with 30 cells along the minor axis of the ellipse. For this mesh size, a maximum error of 2.5 pct was observed when the ellipse image was rotated in relation to the CA mesh (Figure 1(b)).

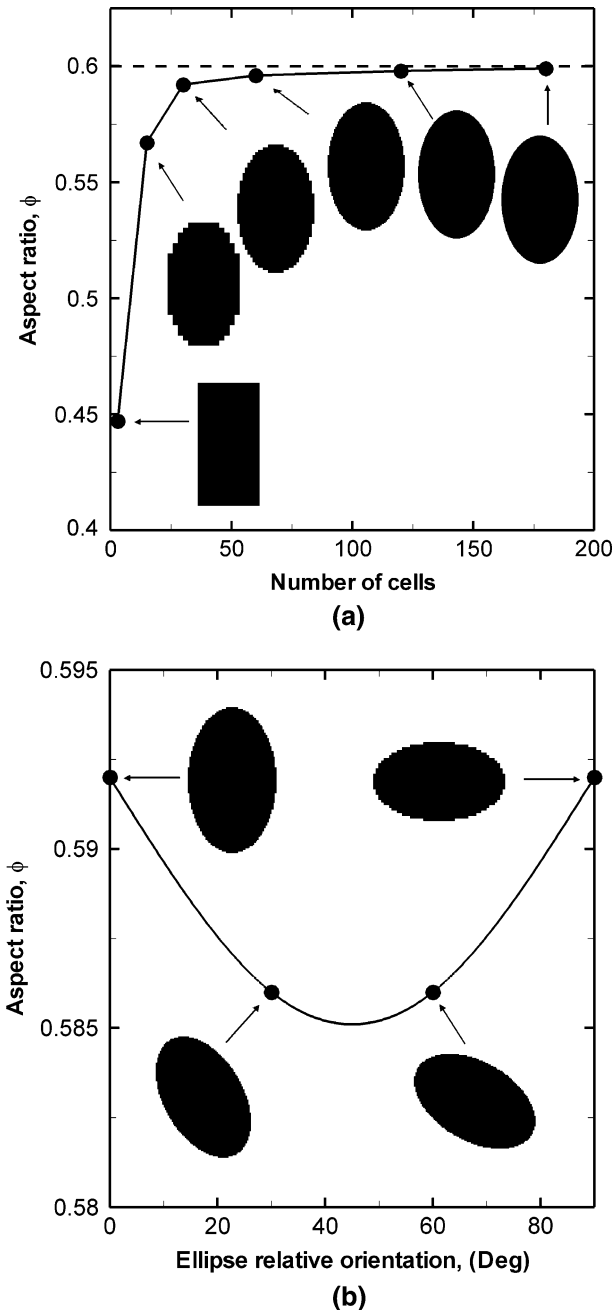


Fig. 1—Calculated aspect ratio ($\phi$) for an ellipse of actual $\phi = 0.6$ as a function of (*a*) number of CA cells along the minor axis and (*b*) orientation of the major axis in relation to the face of the CA cells (considering approximately 30 cells along the minor axis).

The aspect ratio, $\phi$, is evaluated for each grain in the calculated macrostructure. In the direction perpendicular to heat flow, grains have similar $\phi$ owing to the unidirectional solidification conditions of the model. Therefore, to facilitate the definition of a unique CET position, an averaged aspect ratio, $\phi_{av}$, was calculated in the perpendicular direction at a fixed $y$ coordinate. To calculate $\phi_{av}$, each CA cell located at the same $y$ coordinate is given the $\phi$ value of the grain to which it belongs. Then, $\phi_{av}(y)$ is simply an average of all these individual cell $\phi$ values. Finally, a curve of $\phi_{av}$ *vs* $y$ was obtained along several calculated macrostructures, suggesting that when $0 < \phi_{av} < 0.3$, grains are columnar, when $0.4 < \phi_{av} < 1$, grains are equiaxed, and when $0.3 < \phi_{av} < 0.4$, there is a CET region where grains are neither completely columnar, nor completely equiaxed.

Some examples of macrostructures used to define these aspect-ratio ranges are presented in Figure 2. Figure 2(a) shows a macrostructure where the CET position is visually identified very easily. The CET region is relatively narrow, and equiaxed grains clearly have $\phi_{av} > 0.4$. In the macrostructure of Figure 2(b), however, a CET region is not easily visually defined because the CET occurs in a wider region, *i.e.*, the change in grain aspect ratio is more gradual. It is also clear that for $\phi_{av} > 0.4$, grains are equiaxed, and for $\phi_{av} < 0.3$, grains are columnar. In the macrostructure of Figure 2(c), visual identification of the CET is even more difficult. Some elongated grains in the equiaxed region decrease $\phi_{av}$ to almost 0.4. Finally, Figure 2(d) shows a very refined macrostructure, in which the CET is again very difficult to be visually identified. Note that the important feature to obtain the CET position in a macrostructure using the grain aspect ratio is the grain shape, rather than the grain size. Therefore, it is unnecessary to carry out numerous tests of CET identification in macrostructures of different average grain sizes (defined mainly by the number density of grains). The macrostructures in Figure 2 are shown only to illustrate how the method to identify the CET behaves for a set of different grain shapes. The simulation conditions under which they were obtained are completely irrelevant to the present work.

As opposed to the strategy adopted here, in the literature[34–38] the identification of the CET position has always been uniquely based on the visual examination of the grain macrostructures, which, to a large extent, is a subjective process. In the present work, the previous ranges of aspect ratios were defined for the best agreement between the visually identified CET and those obtained from the proposed method. Although this visual identification is still subjective, the proposed method, based on the aspect ratio, is reproducible and always gives the same CET region for the same macrostructure.

The definition of universal ranges of aspect ratio that correctly identify the columnar, equiaxed, and CET regions in all types of macrostructures is not the scope of the present work because these ranges may not even exist. Here, the objective is to show that the aspect ratio can be consistently used to quantitatively define the CET regions in several different types of unidirectionally solidified macrostructures.

## IV. SIMULATION CONDITIONS

The unidirectional solidification of an Al-7 (wt pct) Si alloy was simulated with the three models implemented in the present work. For the solution of the 1-D heat-conduction equation of each model (Eqs. [1] and [4]), the upper boundary ($y = 0.15$ m) was assumed adiabatic, while at the lower boundary

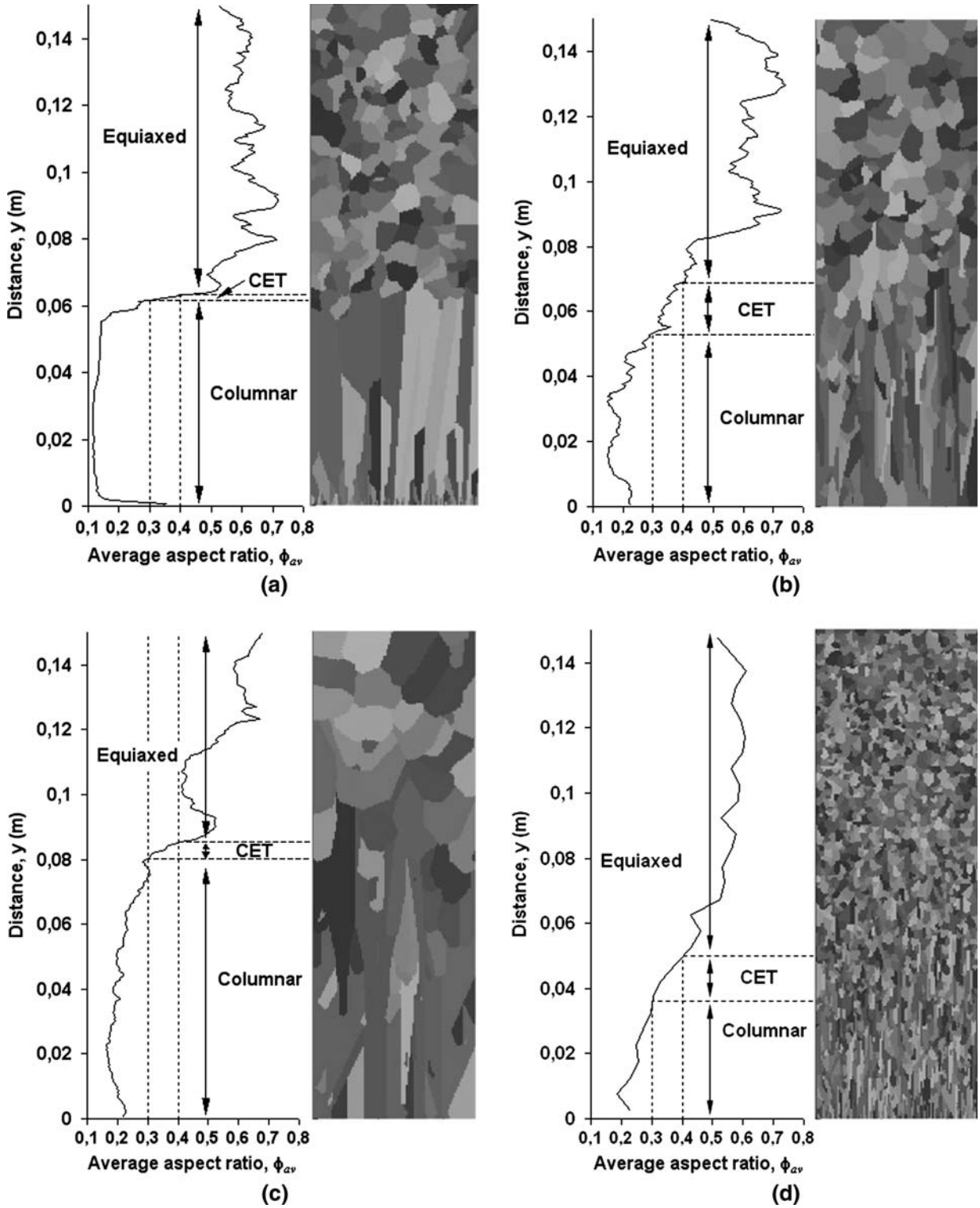


Fig. 2—Average aspect ratio of grains, $\phi_{av}$, along four types of calculated macrostructures, indicating the columnar, equiaxed, and CET regions: (*a*) narrow CET region, (*b*) wide CET region, (*c*) equiaxed region with some elongated grains, and (*d*) very refined macrostructure.

($y = 0$), a heat flux out of the domain was assumed to be $q = h(T - T_\infty)$, where $h$ is the heat-transfer coefficient (250 W m$^{-2}$ K$^{-1}$), and $T_\infty$ is a reference temperature (298 K). A uniform temperature (991 K) was adopted throughout the domain as the initial condition. Despite a few differences relating to ingot size, initial temperature, and heat-transfer coefficient, these simulation conditions are similar to those in the experimental solidification system studied by Gandin.[39]

**Table I. Properties of the Al-7 (Wt Pct) Si Alloy Used in the Simulations**

| Property | Value | Property | Value |
|---|---|---|---|
| $\rho$ (kg m$^{-3}$) | 2452 | $C_0$ (wt pct Si) | 7 |
| $c_p$ (J kg$^{-1}$ K$^{-1}$) | 1126 | $k$ (—) | 0.13 |
| $\kappa_l$ (W m$^{-1}$ K$^{-1}$) | 60.5 | $m_l$ (K pct Si$^{-1}$) | −6 |
| $\kappa_s$ (W m$^{-1}$ K$^{-1}$) | 137.5 | $T_L$ (K) | 891 |
| $L_f$ (J kg$^{-1}$) | $387.4 \times 10^3$ | $T_E$ (K) | 850 |
| $\Gamma$ (m K) | $1.96 \times 10^{-7}$ | $T_f$ (K) | 933 |
| $D_l$ (m$^2$ s$^{-1}$) | $5.5 \times 10^{-9}$ | $n_{T,M}$ (m$^{-2}$) | $3 \times 10^6$ |
| $A$ (m s$^{-1}$ K$^{-m}$) | $3 \times 10^{-6}$ | $\lambda_1$ (mm) | 1.5 |
| $m$ (—) | 2.7 | — | — |

In the stochastic model, $\Delta T_N = 0$ for the substrate particles located in the CA cells adjacent to the mold base ($y = 0$), while different $\Delta T_N$ values were used for the remaining cells, as discussed in Section V. Two types of number density of grains were defined in each simulation: one for the bulk liquid (number of grains per unit volume), $n_{T,B}$ (discussed in Section V), and another for the liquid layer adjacent to the mold base (number of grains per unit area), $n_{T,M}$. These number densities had to be converted to the 2-D CA domain by the following stereological relations:[30] $n_{T,B}^{2D} = \left(n_{T,B}\sqrt{6/\pi}\right)^{2/3}$, and $n_{T,M}^{2D} = 2\sqrt{n_{T,M}/\pi}$.

The constants, $A$ and $m$, in the velocity equation (Eq. [2]) were determined by a nonlinear regression fit to the curve of $V$ *vs* $\Delta T$ calculated with Eq. [7], considering $C_l = C_0$ and $C_d = C_0 - \Delta T/m_l$. Therefore, for the same conditions, Eqs. [2] and [7] give the same growth velocity, allowing a meaningful comparison between the stochastic and deterministic models.

For the numerical solution of the equations of the deterministic model, a 1-D mesh of 200 finite volumes was adopted, as used by Martorano *et al.*[5] For the stochastic model, a 1-D mesh of 30 finite volumes and a 2-D mesh of 300 (heat-flow direction) × 100 (perpendicular to heat flow) CA cells were adopted after numerous refining tests for both the temperature field and the grain macrostructure.

All properties and parameters that were not discussed in the preceding section, but are common to the simulations, are summarized in Table I. The specific parameters for each simulation are discussed in Section V.

## V. COLUMNAR TO EQUIAXED TRANSITION IN DETERMINISTIC AND STOCHASTIC MODELS

The results obtained with the stochastic and the two deterministic models are compared in this section. The microscopic part of the deterministic models is three dimensional because calculations of the growth and volume fraction of the envelopes and of the solute exchange between the envelopes and the extradendritic liquid are all based on 3-D simple shapes, namely, spheres (equiaxed-grain envelopes) and cylinders (columnar-grain envelopes). On the other hand, the microscopic submodel of the stochastic model is two dimensional because it is based on a 2-D mesh of cellular-automaton cells. Nevertheless, stereological relations were used in this model to relate the number density of grains given in three dimensions to that in the 2-D calculation domain. Therefore, the macrostructures obtained with the stochastic model are expected to represent planar sections across 3-D macrostructures, enabling a meaningful comparison between the CET calculated with the stochastic and deterministic models.

### A. *Effects of Nucleation Undercooling and Number Density of Grains*

The CET position was obtained with the three implemented models as a function of $\Delta T_N$ and $n_T$. All models predict an increase in the size of the columnar region for an increase in $\Delta T_N$ (Figure 3(a)), resulting in a completely columnar structure for $\Delta T_N \gtrsim 4$ K. This behavior, shown by Martorano *et al.*[5] for the MBG model, is also observed in the macrostructures calculated with the stochastic model. This comparison between the CET calculated with stochastic and deterministic models has never been shown before.

The columnar region for the MBG model is shorter than that predicted with the MHunt model for a blocking fraction of 0.49. This is in agreement with the CET maps calculated by Martorano *et al.*,[5] which show that the CET of the their model occurs at a higher temperature gradient, corresponding to shorter blocking times and shorter columnar regions in transient unidirectional solidification.

The size of the columnar region predicted by both the MBG and the MHunt models with the traditional columnar-front blocking fraction of 0.49 (MHunt-0.49) is longer than that calculated by the stochastic model. On the other hand, for a blocking fraction of 0.2 (MHunt-0.2), the agreement with the stochastic model improves significantly.

The size of the columnar regions predicted by the three models decreases with increasing $n_T$ (Figure 3(b)), as originally predicted by Hunt's[4] model. The columnar region for the MBG model is again always shorter than the value for the MHunt model (0.49). This difference increases for larger $n_T$, which can also be predicted from the CET map of Martorano *et al.*,[5] because the distance between the transition curves of the two types of models is larger for $n_T = 10^9$ m$^{-3}$ than for $n_T = 10^5$ m$^{-3}$. The size of the columnar region with the MHunt-0.49 is longer than that with the stochastic model, but the agreement is again very good with the Hunt-0.2. This good agreement for several $n_T$ and $\Delta T_N$ values indicates that the blocking that occurs in the stochastic model corresponds closely to the mechanical blocking of the deterministic model by an equiaxed grain fraction of 0.2, rather than 0.49, as proposed by Hunt.[4]

### B. *Columnar Front Undercooling*

The position of the CET is strongly affected by the columnar-front undercooling, which determines the extension of the undercooled liquid ahead of the front,

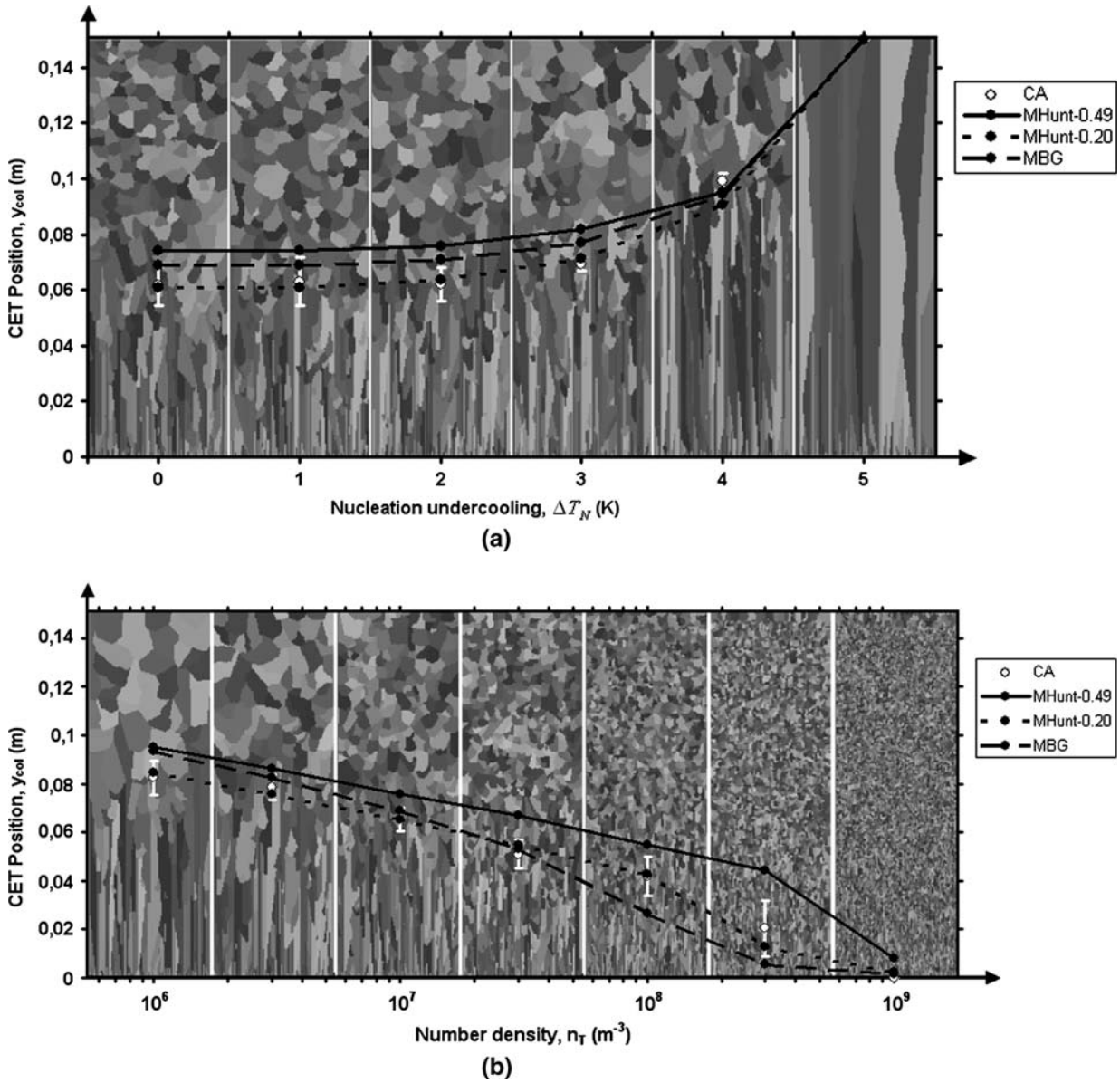


Fig. 3—Macrostructures calculated with the stochastic model (CA) as a function of (*a*) nucleation undercooling, $\Delta T_N$ (for $n_T = 5 \times 10^6\ m^{-3}$) and (*b*) number density of equiaxed grains, $n_T$ (for $\Delta T_N = 3$ K). Also shown is the CET region (obtained from the aspect ratio), outlined by white error bars, and the CET position calculated with the MBG and MHunt models for two different columnar front blocking fractions: 0.49 and 0.2.

where equiaxed grains nucleate and grow.[4] The front undercooling can be obtained for each model using their corresponding temperature field. Several cooling curves extracted from these fields at different distances from the mold base are compared in Figure 4 for the three models, showing good agreement and confirming their correct implementation and identical thermal conditions.

The front undercooling is obtained by interpolating the temperature at the columnar- front position ($y_{col}$) from the temperatures at neighbor finite-volume nodes. In the deterministic model, $y_{col}$ is readily calculated with Eq. [10], whereas in the stochastic model, this position is not clearly identified. Therefore, two possible front positions were defined by examining the simulation domain from the bulk liquid to the solid: (a) the position of the first active CA cell; and (b) the position at which all CA cells in the direction perpendicular to heat flow become active. After defining these two values of $y_{col}$, two columnar-front undercoolings, $\Delta T_{col} = T_L(C_l(y_{col})) - T(y_{col})$, were obtained as a function of time (Figure 5). In the three models, the local liquidus temperature, $T_L$, used to calculate $\Delta T_{col}$, was based on the local $C_l$ concentration, which differs from $C_0$ only in the MBG model.

The curves of $\Delta T_{col}$ for the MBG and the MHunt-0.49 (which was identical to that of the MHunt-0.2 model) models closely agree, indicating a type of steady state in which the undercooling remains approximately constant in the range between 4 and 5 K. This range

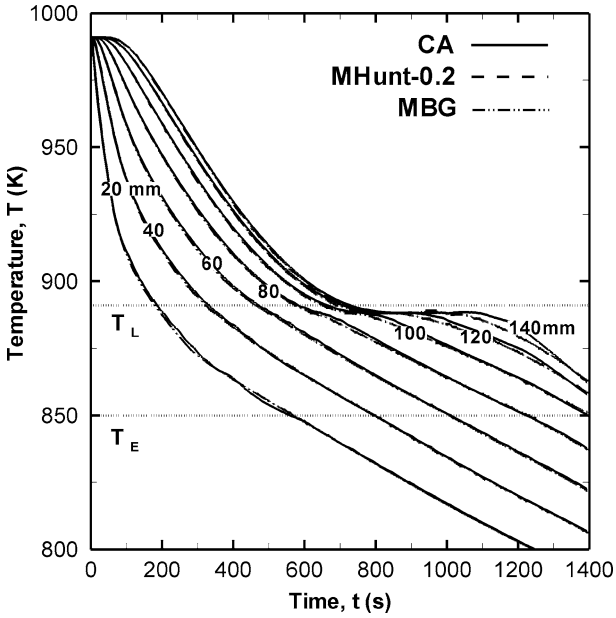


Fig. 4—Cooling curves calculated with the stochastic (CA), MHunt, and MBG models (for $n_T = 5 \times 10^6$ m$^{-3}$ and $\Delta T_N = 3$ K) at different distances from the mold base.

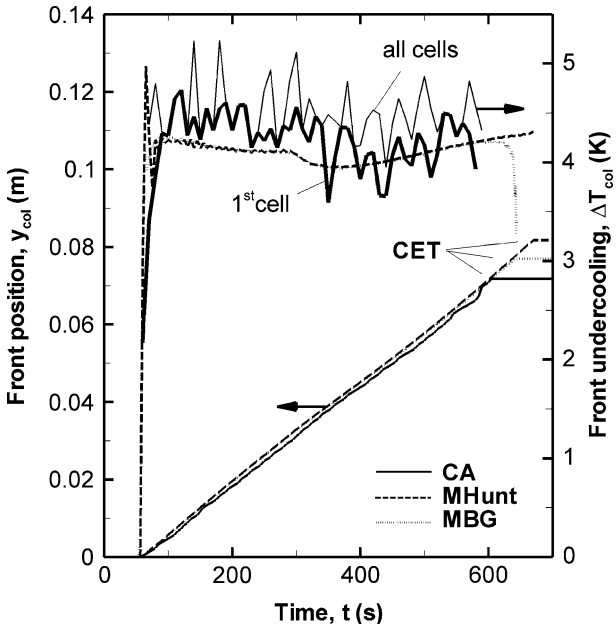


Fig. 5—Columnar-front position ($y_{col}$) and undercooling ($\Delta T_{col}$) for the MBG, MHunt-0.49, and stochastic (CA) models as a function of time (for $n_T = 5 \times 10^6$ m$^{-3}$ and $\Delta T_N = 3$K). For the stochastic model, $\Delta T_{col}$ is given for two definitions of $y_{col}$: one at the position of the first active CA cell (first cell) and the other, where all cells become activated in the direction perpendicular to heat flow (all cells).

was expected from the calculated macrostructures of Figure 3(a), because for $\Delta T_N > 5$ K, no equiaxed grains nucleate ahead of the columnar front. In the MBG model, the undercooling decreases abruptly at the moment of the CET, owing to the solutal-blocking mechanism that results from an increase in $C_l$.[5] The two front-undercooling curves for the stochastic model oscillate around the undercooling curves of the deterministic models. This oscillatory behavior stems from both the discretization of the front position (the front is always located at a cell-site position) and from the fact that the front is determined by the position of several grains of different shapes growing near the front. The undercooling at the front position defined in the stochastic model by the first active CA cell agrees more closely with those from the deterministic models.

Because reasonable agreement is observed between the front-undercooling curves of all three models, the difference in the CET positions is likely to be caused by the different columnar front-blocking mechanisms of each model.

### C. *Geometrical Model for Mechanical Blocking of the Columnar Front*

Solutal blocking of the columnar front occurs when the extradendritic-liquid concentration, $C_l$, increases at the front as a result of the solute transferred from the grain envelopes, removing the undercooling necessary for columnar growth.[5] In contrast, mechanical blocking occurs when there is insufficient space between equiaxed grains for an elongated-grain growth. Hunt[4] suggested that it would occur when the equiaxed-grain volume fraction $\varepsilon_g \geq 0.49$ at the columnar front.

For a relatively small number density of grains, $n_T$, the values of $C_l$ and $\varepsilon_g$ increase almost simultaneously at the columnar front, indicating very similar CET positions for both types of blockings, as shown in Figure 3(b). The CET for the MBG (solutal blocking) and MHunt-0.49 (mechanical blocking) models occurs approximately at similar positions for lower $n_T$. Nevertheless, for a relatively large $n_T$, corresponding to a large envelope interfacial area ($S_e$), the CET occurs earlier for solutal blocking because $C_l$ increases before $\varepsilon_g$ as a result of the intense solute rejection from the envelopes into the extradendritic liquid. Therefore, the columnar region predicted with the MBG model is shorter than that for the MHunt model.

Solutal blocking cannot occur in the stochastic model because solute rejection from grain envelopes into the extradendritic liquid is not taken into account. Therefore, the columnar front should be blocked mechanically, as in the MHunt model; consequently, similar CET positions are expected for the stochastic and MHunt models. Nevertheless, Figure 3(a) and (b) showed that the traditional mechanical-blocking fraction of 0.49 (MHunt-0.49) results in columnar regions that are longer than those predicted by the stochastic model. To derive this blocking fraction, Hunt[4] assumed that the columnar grains would be blocked when the average distance that could be traveled by them (considering the probability of several distances) was shorter than the diameter of the equiaxed grains growing ahead.

In the stochastic model, the columnar front-blocking mechanism was examined in detail in the calculated macrostructures of Figure 6, near the moment of the

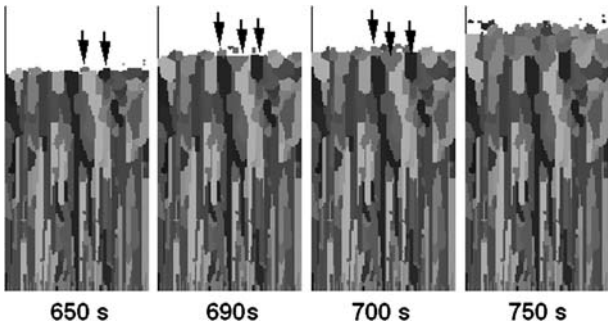


Fig. 6—Detail of macrostructures calculated with the stochastic model during the CET at the indicated times (for $n_T = 5 \times 10^6$ m$^{-3}$ and $\Delta T_N = 3$ K).

CET. At $t = 650$ s, the columnar front is growing upward, and two equiaxed grains indicated by arrows have nucleated at the front. These grains grow laterally at $t = 690$ s, and they virtually impinge on each other at 700 seconds, blocking the growth of a columnar grain below them. Another grain that helps the blocking process is also indicated by an arrow in the macrostructures at $t = 690$ and 700 s. At 750 seconds, a similar type of blocking occurred along the whole columnar front, causing the CET.

A simple geometrical blocking model consistent with the columnar-front blocking observed in Figure 6 is proposed in Figure 7. Because the columnar and equiaxed grains near the front position are approximately at the same temperature, their growth velocities are assumed equal ($V$). The columnar front is blocked when it cannot travel a distance, $R_g$, before two adjacent equiaxed grains impinge on each other, *i.e.*, when the following conditions are met:

$$\frac{R_g}{V} > \frac{R_f - R_g}{V} \qquad [14]$$

where $R_g$ is the instantaneous radius of the equiaxed grains when they contact the columnar front, and $R_f$ is the average half distance between the center of equiaxed grains, which can be calculated approximately by the usual relation, $\frac{R_g}{R_f} = \varepsilon_g^{1/3}$, for a 3-D domain. Substituting this relation into Eq. [14] yields that the columnar front would be blocked when $\varepsilon_g > 0.125$. This fraction is in better agreement (than the traditional 0.49) with that derived from the mechanical blocking of the stochastic model ($\varepsilon_g = 0.2$). One reason that can be attributed to the remaining discrepancy is that equiaxed grains were assumed to grow with the same velocity in all directions in Figure 7, while in the stochastic model, there are four preferential directions of growth, and these are not generally parallel to the columnar-front line.

## VI. SUMMARY AND CONCLUSIONS

Two deterministic models and one stochastic model have been implemented to investigate the mechanical blocking of the columnar front that leads to the CET in the unidirectional solidification of an Al-7 pct Si alloy.

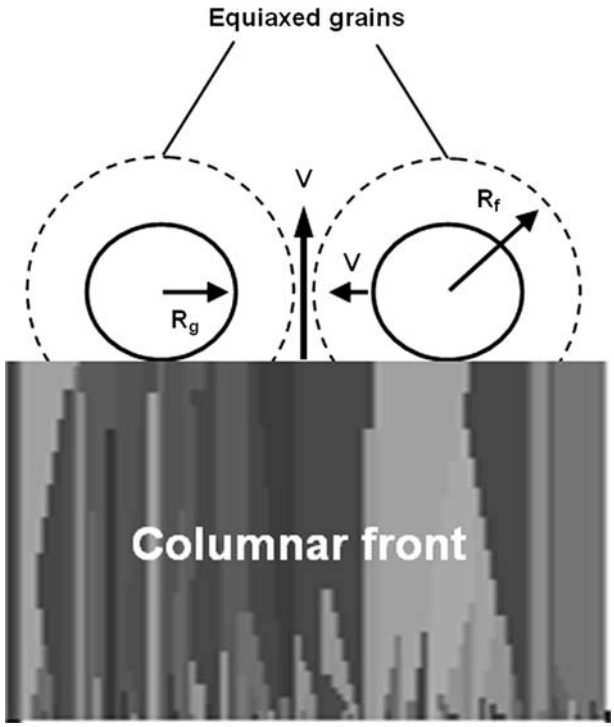


Fig. 7—Geometrical model for the mechanical blocking of the stochastic model.

Each deterministic model is based on a different type of mechanism that blocks the front: the Martorano *et al.*[5] model (MBG) is based on the solutal blocking, and the modified Hunt[4] model (MHunt) is based on the mechanical blocking. To quantitatively compare, for the first time, the CET positions obtained with the three models, a special procedure considering the aspect ratio of grains has been developed to determine the location of the CET in the macrostructures of the stochastic model.

The size of the columnar zones obtained with both the MBG and the MHunt model for the traditional blocking-grain fraction of $\varepsilon_g = 0.49$ (MHunt-0.49) is always larger than that predicted with the stochastic model. Nevertheless, for a fraction of $\varepsilon_g = 0.2$ (MHunt-0.2), the agreement improves significantly in a wide range of number density of grains and nucleation undercoolings. This indicates that the mechanical blocking that occurs in the stochastic model can be simulated in the deterministic model by adopting a blocking fraction of $\varepsilon_g = 0.2$, rather than the 0.49 suggested by Hunt.[4] Finally, a simple geometrical model has been proposed for the mechanical blocking, yielding a blocking fraction of 0.125.

## ACKNOWLEDGMENTS

The authors thank Fundação de Amparo à Pesquisa do Estado de São Paulo (Grant No. 03/08576-7) and Conselho Nacional de Desenvolvimento Científico e Tecnológico (Grant No. 475451/04-0) for the financial support and the scholarship to V.B. Biscuola.

## REFERENCES


1. S.C. Flood and J.D. Hunt: *ASM Handbook*, ASM, Materials Park, OH, 1998, vol. 15, pp. 130–36.
2. D. StJohn and J. Hutt: *Int. J. Cast Met. Res.*, 1998, vol. 11, pp. 13–22.
3. H. Nguyen-Thi, G. Reinhart, N. Mangelinck-Noel, H. Jung, B. Billia, T. Schenk, J. Gastaldi, J. Hartwig, and J. Baruchel: *Metall. Mater. Trans. A*, 2007, vol. 38A, pp. 1458–64.
4. J.D. Hunt: *Mater. Sci. Eng.*, 1984, vol. 65, pp. 75–83.
5. M.A. Martorano, C. Beckermann, and C.A. Gandin: *Metall. Mater. Trans. A*, 2003, vol. 34A, pp. 1657–74.
6. S.C. Flood and J.D. Hunt: *J. Cryst. Growth*, 1987, vol. 82, pp. 543–51.
7. S.C. Flood and J.D. Hunt: *J. Cryst. Growth*, 1987, vol. 82, pp. 552–60.
8. C.Y. Wang and C. Beckermann: *Metall. Mater. Trans. A*, 1994, vol. 25, pp. 1081–93.
9. M.A. Martorano and V.B. Biscuola: *Model. Simul. Mater. Sci. Eng.*, 2006, vol. 14, pp. 1225–43.
10. A. Jacot, D. Maijer, and S. Cockcroft: *Metall. Mater. Trans. A*, 2000, vol. 31A, pp. 2059–68.
11. R.H. Mathiesen and L. Arnberg: *Mater. Sci. Eng. A*, 2005, vol. 413, pp. 283–87.
12. R.H. Mathiesen, L. Arnberg, P. Bleuet, and A. Somogyi: *Metall. Mater. Trans. A*, 2006, vol. 37A, pp. 2515–24.
13. A. Ludwig and M. Wu: *Mater. Sci. Eng. A*, 2005, vol. 413, pp. 109–14.
14. A. Ciobanas, F. Baltaretu, and Y. Fautrelle: *Solidification and Gravity Iv*, 2006, vol. 508, pp. 239–44.
15. D.J. Browne: *ISIJ Int.*, 2005, vol. 45, pp. 37–44.
16. J. Banaszek, S. McFadden, D.J. Browne, L. Sturz, and G. Zimmermann: *Metall. Mater. Trans. A*, 2007, vol. 38A, pp. 1476–84.
17. S. McFadden and D.J. Browne: *Scripta Mater.*, 2006, vol. 55, pp. 847–50.
18. D.J. Browne and J.D. Hunt: *Numer. Heat Transfer B-Fund.*, 2004, vol. 45, pp. 395–419.
19. J.A. Spittle and S.G.R. Brown: *J. Mater. Sci.*, 1989, vol. 24, pp. 1777–81.
20. C.A. Gandin and M. Rappaz: *Acta Mater.*, 1997, vol. 45, pp. 2187–95.
21. M. Rappaz, C.A. Gandin, J.L. Desbiolles, and P. Thevoz: *Metall. Mater. Trans. A*, 1996, vol. 27A, pp. 695–705.
22. H.B. Dong and P.D. Lee: *Acta Mater.*, 2005, vol. 53, pp. 659–68.
23. I.S. Cho and C.P. Hong: *ISIJ Int.*, 1997, vol. 37, pp. 1098–106.
24. R.C. Atwood, P.D. Lee, R.S. Minisandram, and R.M.F. Jones: *J. Mater. Sci.*, 2004, vol. 39, pp. 7193–97.
25. A. Kermanpur, N. Varahram, P. Davami, and M. Rappaz: *Metall. Mater. Trans. B*, 2000, vol. 31B, pp. 1293–1304.
26. D.R. Liu, J.J. Guo, S.P. Wu, Y.Q. Su, and H.Z. Fu: *Mater. Sci. Eng. A*, 2006, vol. 415, pp. 184–94.
27. M. Wu and A. Ludwig: *Metall. Mater. Trans. A*, 2007, vol. 38A, pp. 1465–75.
28. S.V. Patankar: *Numerical Heat Transfer and Fluid Flow*, Hemisphere Publishing Corp., New York, NY, 1980, pp. 54–59.
29. C.A. Gandin and M. Rappaz: *Acta Metall. Mater.*, 1994, vol. 42, pp. 2233–46.
30. M. Rappaz and C.A. Gandin: *Acta Metall. Mater.*, 1993, vol. 41, pp. 345–60.
31. P. Thevoz, J.L. Desbiolles, and M. Rappaz: *Metall. Trans. A*, 1989, vol. 20A, pp. 311–22.
32. J. Lipton, M.E. Glicksman, and W. Kurz: *Mater. Sci. Eng.*, 1984, vol. 65, pp. 57–63.
33. T. Allen: *Particle Size Measurement*, Chapman & Hall, London, 1997, pp. 112–55.
34. C.A. Gandin: *Acta Mater.*, 2000, vol. 48, pp. 2483–2501.
35. M.A. Martorano and J.D.T. Capocchi: *Int. J. Cast. Met. Res.*, 2000, vol. 13, pp. 49–57.
36. C.A. Siqueira, N. Cheung, and A. Garcia: *J. Alloys Compd.*, 2003, vol. 351, pp. 126–34.
37. R.B. Mahapatra and F. Weinberg: *Metall. Trans. B*, 1987, vol. 18B, pp. 425–32.
38. I. Ziv and F. Weinberg: *Metall. Trans. B*, 1989, vol. 20B, pp. 731–34.
39. C.A. Gandin: *ISIJ Int.*, 2000, vol. 40, pp. 971–79.